Land Degradation Assessment Applying Different Methods for Soil Erosion Estimation

Christos Pantazis and Panagiotis Nastos *

Posted Date: 16 March 2026

doi: 10.20944/preprints202603.1172.v1

Keywords: soil erosion; land degradation; RUSLE; DEM of Difference; field measurements; Mediterranean olive groves; Messenia; Greece

 doi:10.20944/preprints202603.1172.v1

Article

Land Degradation Assessment Applying Different Methods for Soil Erosion Estimation

Christos Pantazis [1,2,3] and Panagiotis Nastos [1,4,*]

[1] Department of Geology and Geoenvironment, National and Kapodistrian University of Athens, 15784, Athens, Greece

[2] Research Centre of Atmospheric Physics and Climatology, Academy of Athens, 10680, Athens, Greece

[3] Navarino Environmental Observatory (N.E.O.), 24001 Messenia, Greece

[4] Biomedical Research Foundation of the Academy of Athens, 11527 Athens, Greece

* Correspondence: nastos@geol.uoa.gr

Abstract

Land degradation caused by soil erosion is a major challenge in Mediterranean sloped agroecosystems, where extreme weather events and conventional land management practices accelerate soil loss and threaten long-term sustainability. This study evaluates and compares three complementary approaches to estimate soil erosion in an olive orchard in Messenia, Greece. Field-based runoff plots provided direct measurements of sediment yield, drone-based LiDAR surveys enabled soil surface change detection through the Difference of Digital Elevation Models (DoD) method, and the Revised Universal Soil Loss Equation (RUSLE) was applied to model erosion risk using site-specific parameters. Results indicate that field measurements and RUSLE estimates are broadly consistent, particularly when the model is calibrated with empirical data, offering reliable insights into soil loss dynamics. In contrast, the LiDAR–DoD approach was used to characterize soil surface displacement rather than to directly quantify soil erosion. Due to methodological and technical limitations, LiDAR–DoD results are presented primarily as a framework for future research rather than as a definitive erosion assessment tool. Overall, the integration of field monitoring, remote sensing, and modeling highlights the strengths and limitations of each method and demonstrates the value of multi-method approaches for improving erosion assessment and supporting sustainable land management in vulnerable Mediterranean landscapes.

Keywords: soil erosion; land degradation; RUSLE; DEM of Difference; field measurements; Mediterranean olive groves; Messenia; Greece

1. Introduction

Soil erosion by water is one of the most important forms of land degradation, affecting soil fertility [1], agricultural productivity [2], water quality [3], and ecosystem stability worldwide [4]. It is especially critical in Mediterranean environments, where steep topography, intense seasonal rainfall, sparse vegetation cover during part of the year, and long-term agricultural use create favorable conditions for runoff generation and soil detachment [5–7]. In these landscapes, erosion is not only a geomorphological process but also a major environmental and socio-economic issue, because it reduces the productive capacity of soils and contributes to the progressive degradation of cultivated land [8,9]. Olive-growing areas are particularly relevant in this context, as they represent one of the dominant land uses in many Mediterranean regions and are often located on sloping terrain that is vulnerable to erosion [7,10].

The Mediterranean climate is characterized by a strong seasonal contrast, with dry summers and rainfall concentrated mainly in autumn and winter [11]. Under these conditions, the erosive impact of rainfall is often intensified by the limited protective cover of the soil surface at the beginning of the rainy season. In many olive orchards, especially those managed conventionally, the soil between tree

 doi:10.20944/preprints202603.1172.v1

rows may remain bare or only partly covered for long periods, increasing its exposure to raindrop impact and overland flow [12]. Repeated tillage, low organic matter content, and inadequate conservation practices may further increase soil susceptibility to erosion [13,14]. As a result, Mediterranean olive groves have frequently been identified as high-risk areas for soil degradation, sediment redistribution, and long-term decline in soil quality [15].

Because soil erosion is controlled by the interaction of multiple factors, including rainfall, soil properties, slope, vegetation cover, and land management, its assessment remains methodologically challenging. No single approach can fully capture all dimensions of the process. Direct field measurements provide valuable information on actual soil loss under real conditions, but they are often limited to small plots and specific time periods [16]. Empirical models, on the other hand, make it possible to estimate erosion over larger areas and to explore its spatial distribution, although their reliability depends strongly on the quality of the input data and on local validation [17]. In recent years, high-resolution topographic techniques such as LiDAR and photogrammetry have added a new dimension to erosion studies by allowing the detection of subtle changes in surface elevation and local redistribution patterns [18]. These different approaches are therefore complementary rather than interchangeable.

Among the empirical approaches available for soil erosion estimation, the Revised Universal Soil Loss Equation (RUSLE) is one of the most widely applied models [19]. RUSLE estimates average annual soil loss based on rainfall erosivity, soil erodibility, topographic characteristics, land cover, and conservation practices [20]. Its widespread use is related to its relatively simple structure, modest data requirements compared with more physically based models, and compatibility with GIS-based spatial analysis [21]. For this reason, RUSLE has been used extensively in watershed studies, agricultural landscapes, and erosion risk mapping applications. However, its use also requires caution. Since RUSLE is an empirical model, its predictions depend heavily on the representativeness and spatial accuracy of the input factors, and its application is more robust when supported by local information and field observations. Validation is therefore essential if model outputs are to be interpreted with confidence [22].

At the same time, field experiments remain one of the most direct ways to quantify real soil loss from a defined area. Measurements obtained from monitored plots can provide useful evidence of temporal variability and event-driven erosion, particularly in cultivated systems where soil loss may occur in short pulses associated with rainfall episodes [16]. Such data are particularly valuable because they offer an empirical basis against which model results can be compared. Nevertheless, field measurements alone cannot describe the spatial distribution of erosion beyond the monitored plot, nor can they easily reveal how sediment is redistributed across the surface [23]. This limitation has encouraged the integration of field observations with spatial models and terrain-based techniques.

In this context, LiDAR-derived digital elevation models (DEMs) and DEM of Difference (DoD) analysis provide an additional tool for investigating soil surface dynamics at very fine scales. By comparing elevation models acquired at different times, DoD analysis can identify areas of local surface lowering and raising, thereby helping to describe short-term terrain change and soil redistribution [24]. While this method does not necessarily measure soil loss directly, it is particularly useful for visualizing surface behaviour and the movement of material within small experimental plots. As such, it can complement both direct field measurements and model-based predictions by adding information on local microtopographic change.

The present study was developed within this broader methodological context and aimed to assess soil erosion in a Mediterranean olive-growing sub-catchment in southwestern Greece using a combination of approaches. More specifically, the study integrates: (i) direct field measurements of soil loss from an experimental subplot, (ii) spatial estimation of soil erosion using the RUSLE model, and (iii) LiDAR- and DoD-based analysis of short-term surface elevation changes. The decision to focus on a small, well-defined sub-catchment was made to improve the spatial reliability of the RUSLE application and to allow direct comparison between model outputs and field observations at

 doi:10.20944/preprints202603.1172.v1

the location of the experimental plot. This design also makes it possible to examine how different methods perform when applied to the same erosion-prone environment.

The main objective of the study is therefore not only to estimate soil erosion, but also to evaluate the extent to which these different methodologies provide consistent and complementary information. By combining direct measurement, empirical modelling, and high-resolution terrain analysis, the study seeks to contribute to a more holistic understanding of soil erosion and land degradation processes in Mediterranean agroecosystems. Such an integrated approach is important for improving erosion assessment, supporting model validation, and informing more effective soil conservation and sustainable land management strategies in vulnerable cultivated landscapes.

2. Materials and Methods

The study was carried out in a sub-catchment of the Xerias River watershed in the Pylos–Nestor area of Messenia, southwestern Greece (Figure 1). Although the broader Xerias watershed covers a much larger area, the present analysis focused on a smaller section that was selected according to local topographic which defines a clear and practical boundary for modelling purposes. This smaller unit was considered appropriate for the application of the RUSLE model, since it includes the experimental plots used in the field study and represents the terrain conditions most relevant to the objectives of this work.

The landscape is typical of Mediterranean environments, with gentle to moderately sloping terrain, small drainage pathways, and agricultural land mixed with patches of natural vegetation. The dominant land use in the area is olive cultivation, accompanied by shrubland and scattered woodland vegetation. Soils are mainly calcareous Mediterranean soils, generally ranging from loam to clay loam, and they have a moderate to relatively high susceptibility to erosion, especially where vegetation cover is limited.

The climate of the region is Mediterranean, with rainfall concentrated mainly in the wet season from autumn to spring, while summers are hot and dry [25,26]. Under these conditions, soil loss is strongly influenced by seasonal rainfall intensity, slope, land cover, and management practices [14]. Even though the selected sub-catchment is relatively small compared to the entire Xerias watershed, it provides a representative and well-defined area for investigating erosion processes at the local scale.

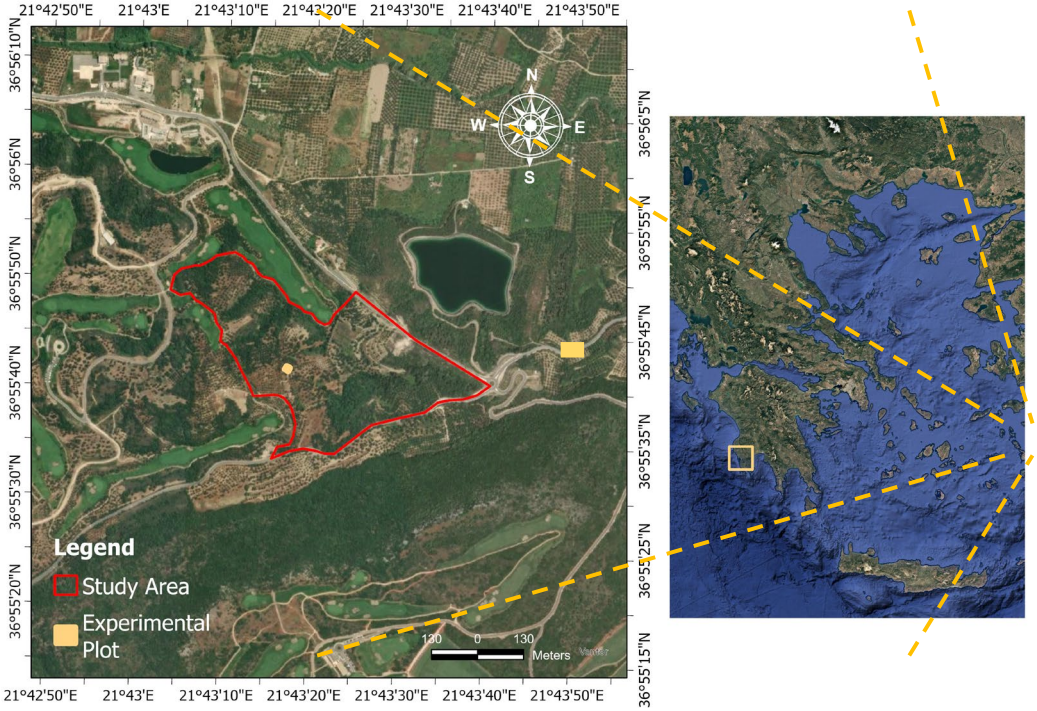

 doi:10.20944/preprints202603.1172.v1

Figure 1. Location of the study area in a sub-catchment of the Xerias River watershed, Pylos–Nestor, Messenia, Greece.

2.1. Field Monitoring of Runoff and Sediment

To anchor the modelling in empirical evidence under local orchard conditions, we used runoff and sediment data from the field experiment developed by [27]. The experiment employed bounded runoff plots that route surface runoff and associated sediment to a collector and storage tanks, enabling event-scale quantification of runoff volume and sediment yield. Such plots are widely used in Mediterranean olive systems to measure gross soil loss and compare management practices, although known scale and border effects should be considered when interpreting results [7].

In the full experimental design, nine plots (10 m × 10 m) were established on a representative hillslope within an olive grove as three treatments with three replicates. In the present study, we report and analyse data from one plot corresponding to the herbicide treatment (one of the nine plots). The plot was located on a slope segment with a mean gradient of ~16% and was equipped at its downslope boundary with (a) a collection channel/trough spanning the plot width and (b) a sealed storage tank positioned downslope to retain runoff and sediment from each rainfall event (Figure 2). This configuration follows standard plot-collection principles for erosion experiments, including ensuring free discharge into the tank and sufficient storage capacity for infrequent high-magnitude storms.

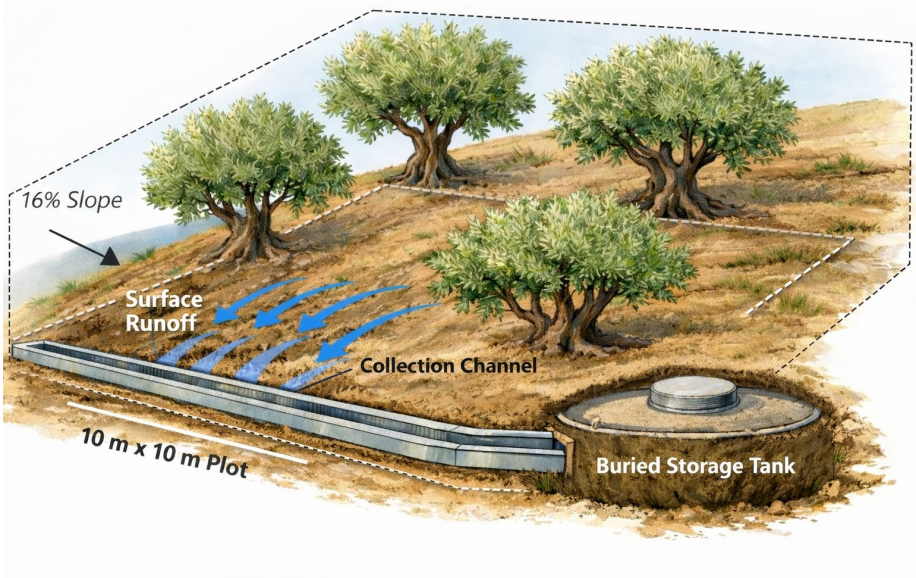

Figure 2. Experimental set up of the soil erosion monitoring network.

After each major rainfall event, total runoff volume was measured from the tank. The sediment-laden water was then processed to estimate event sediment yield: deposited material was re-suspended and sub-sampled or fully recovered as appropriate, and sediment was oven-dried to constant mass before weighing, following standard plot-scale water erosion protocols. Event soil loss was calculated as dry sediment mass divided by plot area and reported in t ha^{-1} $event^{-1}$, with seasonal totals obtained by summing events over the monitoring period (typically October–April in Mediterranean climates). These measurements were used to (i) document the magnitude and temporal variability of erosion under the herbicide-managed orchard condition and (ii) provide an external check on whether GIS-based RUSLE predictions fall within a plausible local range at the hillslope scale.

2.2. RUSLE Framework and GIS Implementation

 doi:10.20944/preprints202603.1172.v1

Spatial modelling was conducted using the RUSLE multiplicative structure:

$$A = R * K * LS * C * P \quad (1)$$

where A is average annual soil loss (long-term mean) from rill and interrill processes, R is rainfall erosivity, K is soil erodibility, LS is the combined slope length and slope steepness factor, C is the cover-management factor, and P is the support practice factor [28].

All these factors affect soil loss [20], and the layers were prepared as gridded rasters at a consistent 5 m spatial resolution, aligned to a common projection and extent. The rasters were then combined using cell-by-cell multiplication to generate a continuous soil loss surface across the study sub-catchment. The GIS workflow followed (Figure 3) standard map-algebra practice: (i) preprocess primary inputs (rainfall data, soil properties, DEM, and land cover), (ii) derive R, K, LS, C, and P layers with consistent units and scaling, and (iii) compute A from their product [29].

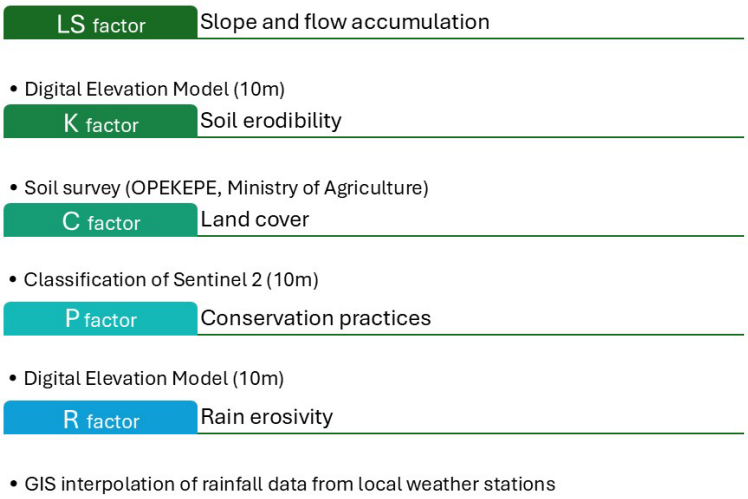

Figure 3. Workflow of RUSLE model.

Because RUSLE predicts long-term average annual soil loss rather than event sediment delivery at the catchment outlet, outputs were interpreted as gross erosion potential (sheet and rill) at the hillslope scale. Measured plot erosion therefore provides a valuable consistency check but is not expected to match model output perfectly, especially when plot monitoring covers a single season and when local deposition or rill initiation thresholds operate [19].

2.2.1. Rainfall Erosivity Factor Calculation

Rainfall erosivity represents the erosive power of rainfall and its capacity to generate runoff capable of detaching and transporting soil. According to [28], erosivity is derived from rainfall intensity metrics (e.g., EI30), but such high-frequency records are often unavailable for many Mediterranean monitoring networks. As an alternative, erosivity can be approximated from precipitation totals aggregated at monthly or annual scales [30].

In this study, R was derived from the modified Fournier framework described by [31] which documents [32] Fournier's original precipitation concentration index to improve correlation with erosivity. For each station, daily rainfall records were aggregated to monthly totals and annual totals. The modified Fournier index (MFI) was computed as:

$$\mathrm{MFI} = \frac{\Sigma_1^{12} \mathrm{P_i^2}}{\mathrm{P}} \quad (2)$$

where Pi is precipitation for month i and P is annual precipitation.

Following the relationship reported by [33], erosivity was estimated as:

 doi:10.20944/preprints202603.1172.v1

$$R = 0.264\ MFI^{1.50} \quad (3)$$

This precipitation-based erosivity approach is explicitly recommended for application within homogeneous climatic settings, because the F-R relationship can vary across rainfall regimes [30]. Accordingly, a station network (Figure 4) of 4 rain gauges was selected to represent the same regional climatic domain as the target sub-catchment, and multi-year averaging (2016-2025) was performed to suppress single-year anomalies and better approximate long-term erosive forcing.

Station-level R values were then interpolated across the catchment to generate a continuous erosivity raster at 5 m resolution. Interpolation was performed with a distance-weighted method appropriate to station density and topographic variability, and the resulting raster was clipped to the study-area boundary. The resulting R map was treated as time-invariant for the modelling period, consistent with the long-term average nature of RUSLE.

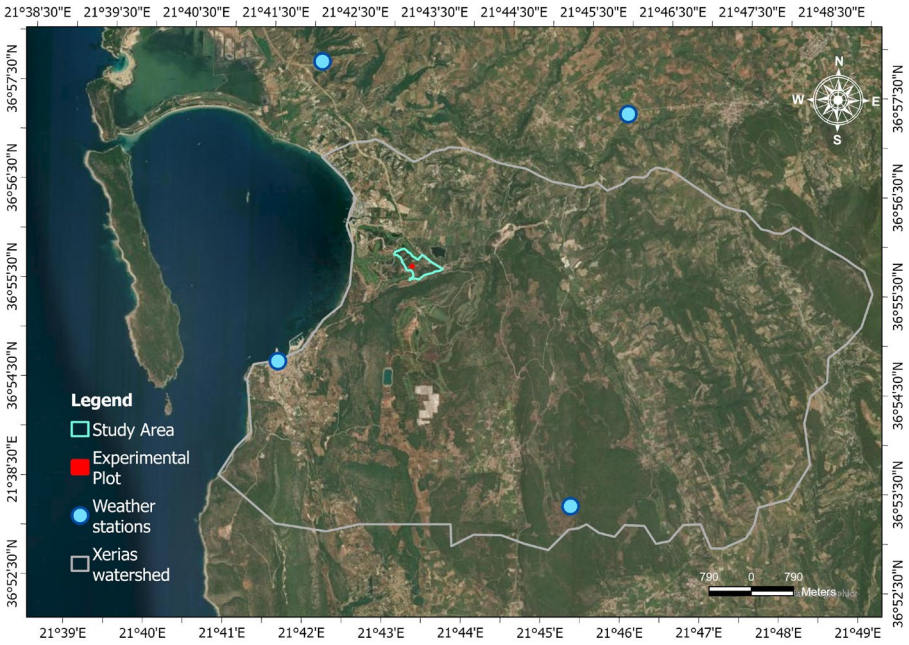

Figure 4. Weather station network.

2.2.2. Soil Erodibility Factor Calculation

Soil erodibility K describes how easily soil can be detached and carried away by rainfall and runoff under standard reference conditions. It mainly depends on soil texture, organic matter, structure, and how quickly water can move through the soil [29]. K is usually estimated either from standard-plot measurements or from equations that relate K to measured soil properties (pedotransfer methods).

In this study, the required soil inputs (soil texture, organic matter, soil-structure class, and permeability class) were obtained from the OPEKEPE open soil datasets (Ministry of Rural Development and Food). These spatial layers were used to parameterize the K-factor across the study sub-catchment, ensuring consistent coverage and attribute definitions across land-cover units. To confirm that the mapped properties were representative locally, the OPEKEPE values were validated using field observations and laboratory analyses from soil samples collected at the experimental plot. Agreement was then checked for texture class, organic matter levels, and the assigned structure and permeability classes.

The erodibility factor was computed using the widely cited algebraic approximation of the original USLE nomograph developed by [28,29] and reported in metric-converted form (including the 0.1317 unit conversion multiplier [19]) in authoritative documentation. The equation applied was:

 doi:10.20944/preprints202603.1172.v1

$$K = 0.1317 \times (2.1 \times M^{-1.14} \times 10^{-4} \times (12 - a) + 3.25(b - 2) + 2.5(c - 3))/100 \quad (4)$$

where M is the texture term M = ($m$silt + $m$vfs) (100 − mc), with $m$silt = percent silt, $m$vfs = percent very fine sand, and mc = percent clay; OM is organic matter (%); s is the soil-structure class code; and p is the permeability class code.

A catchment-wide K raster at 5 m resolution was generated by linking computed K values to mapped soil units. The approach ensured that K varied spatially according to dominant soil property patterns while maintaining physical plausibility (e.g., higher K in fine-textured, low-OM soils). This aligns with the conceptual interpretation of K as a soil-property-controlled modifier of erosion susceptibility in RUSLE-type formulations.

2.2.3. Topographic and Management Factors

Topography strongly affects erosion because it controls how runoff concentrates and how much energy the flowing water has. In GIS, slope-length effects are often represented using upslope contributing area (the area draining into each cell). This lets the LS factor reflect flow convergence and divergence on complex terrain instead of assuming a uniform hillslope. Accordingly, the combined LS factor was computed using a unit stream power / contributing-area formulation linked to [34].

$$LS = (As/22.13)^m \times (\sin\beta /0.0896)^n \quad (5)$$

where As is the specific catchment area (upslope contributing area per unit contour width), β is the slope angle, m = 0.4 and n = 1.3.

A hydrologically corrected DEM was used to compute flow direction, flow accumulation, and slope. The contributing-area term As was derived by combining flow accumulation with grid-cell size (i.e., converting accumulated cell counts to contributing area per unit width), while slope was computed in degrees and converted as required for trigonometric functions. This approach captures how runoff concentrates in converging areas of the terrain, which is a key advantage formulation compared with methods that represent slope length only [35].

2.2.4. Cover-Management Factor

Vegetation and management reduce soil loss by shielding the soil from raindrop impact, increasing hydraulic roughness, and improving infiltration. In RUSLE, this is captured by the cover-management factor C.

Land cover in the study sub-catchment was mapped into a small number of dominant classes that reflect the local landscape (olive groves, sclerophyllous vegetation, and mixed agricultural land with significant natural vegetation). Because the sub-catchment is small and well known, the classification was produced using local knowledge and detailed interpretation. values for each class were assigned from published literature values reported by [36]. In particular, the following values were used:

Table 1. C-factor per cover type.

Land cover	C-factor
Olive groves	0.2273
Sclerophyllous vegetation	0.0623
Land principally occupied by agriculture with significant areas of natural vegetation	0.1232

2.2.5. Support Practice Factor

 doi:10.20944/preprints202603.1172.v1

The support practice factor (P) accounts for how conservation measures (e.g., contouring, strip cropping, terraces) can reduce erosion compared with straight up-and-down-slope conditions. Because detailed parcel-scale information on these practices was not available across the whole sub-catchment, P was estimated using a simple slope-based relationship [28] that is commonly used in GIS-RUSLE studies when practice inventories are limited:

$$P = 0.2 + 0.03 \times S \quad (6)$$

where S is sloping gradient expressed as percent.

In the GIS implementation, P values were limited to the normal range of the factor (0-1), so that P does not increase erosion above the no-practice baseline. This produces a spatial P surface that increases with slope, reflecting that conservation practices are generally less effective on steeper terrain when other conditions are similar.

2.3. DEMs of Difference Methodology

DoD methodology was applied to describe the soil movement within the subplots. Having as a benefit the LiDAR sensor we can remove vegetation including olive trees and detect soil behavior during a long period with precipitation. Repeat UAV-LiDAR surveys were conducted to derive spatially explicit erosion/deposition estimates. Data acquisition used a DJI Matrice 300 RTK platform carrying a DJI Zenmuse L2 LiDAR payload. The Zenmuse L2 integrates LiDAR with a high-accuracy IMU and supports multi-return acquisition (capturing up to five return signals from each laser pulse). In orchard environments, tree crowns and ground vegetation can partially block the soil surface in image-based reconstructions. Multi-return LiDAR increases the likelihood of obtaining ground observations through canopy gaps [37]. In contrast, UAV photogrammetry may fail to reconstruct "dead ground" beneath vegetation because it relies on optical visibility [38].

Two surveys were carried out at the beginning of December 2024 and in early May 2025, and each point cloud was processed to generate a gridded DEM at 0.05 m resolution. Point-cloud reconstruction and terrain modelling were performed in DJI Terra. Ground elevations were not derived simply by selecting the "last return." Instead, a ground-point classification procedure was applied to distinguish bare-earth points from vegetation and other objects. DJI Terra's dedicated ground-classification workflow was used, with terrain-dependent parameter settings, to generate the DEM from the classified ground points. This distinction matters because ground filtering/classification is a recognized source of uncertainty in terrain modelling under canopy and on complex slopes.

Topographic change between the two dates was quantified using a DEM-of-Difference (DoD):

$$DoD = DEM\_May2025 - DEM\_Dec2024 \quad (7)$$

Following this definition, negative DoD values represent elevation loss (surface lowering/erosion) and positive values represent deposition. The DoD approach is widely used for morphological sediment budgets but requires attention to survey/model uncertainty and the possibility that apparent changes reflect noise rather than geomorphic signal [39]. DoD values (Δz, m) were converted to per-cell volumes using the grid-cell area:

$$\Delta V_i = \Delta z_i \times A \quad (8)$$

where $A = 0.05\ m \times 0.05\ m = 0.0025\ m^2$.

Summing ΔV_i across all cells yielded the net volumetric change (m^3) over the observation period. Net volume was then converted to mass using the measured average bulk density from the plot (ϱb = 1.1 g cm^{-3}, equivalent to 1.1 t m^{-3} by unit conversion), giving

$$M = V \times \varrho b\ (t) \quad (9)$$

Finally, DoD-derived net mass change was compared against sediment masses obtained from the runoff-plot collection system. This comparison should be interpreted carefully because DoD

 doi:10.20944/preprints202603.1172.v1

measures net elevation changes within the mapped area (erosion minus deposition), whereas outlet sediment represents exported material, which can diverge when substantial within-plot redistribution or temporary storage occurs.

3. Results

3.1. Field-Based Measurements of Soil Loss

Direct measurements collected in the 100 m² experimental subplot revealed marked temporal variability in soil loss during the two monitoring periods. In the 2023-2024 period (Figure 5a), the highest measured values were recorded at the beginning of the observation period, reaching 2875 g/100 m² on 11 October and 1554 g/100 m² on 19 October. After these initial peaks, soil loss declined substantially, with later measurements showing much lower values of 264 g/100 m², 52 g/100 m², 40 g/100 m², and 188 g/100 m². The cumulative measured soil loss for this monitoring year was 4973 g/100 m², which corresponds to 0.497 t ha^{-1} yr^{-1}. However, the total results from the first monitoring year should be interpreted with some caution, as technical problems during field data collection resulted in gaps in the measurement series. As a result, the available dataset for 2023-2024 does not provide a fully continuous record of soil loss throughout the whole monitoring period, and some intermediate events may not have been captured.

In contrast, the 2024-2025 monitoring period (Figure 5b) provides a more complete record of the temporal dynamics of direct soil loss in the subplot. During this second year, soil loss values showed strong fluctuations between measurement dates, ranging from 65 g/100 m² to 2330 g/100 m². Several pronounced peaks were recorded during the winter period, particularly on 7 December (963 g/100 m²), 20 December (2330 g/100 m²), 14 January (1380 g/100 m²), and 28 January (890 g/100 m²), while lower but still notable values were observed on the remaining dates. The cumulative measured soil loss for 2024-2025 reached 7676 g/100 m², equivalent to 0.768 t ha^{-1} yr^{-1}. Overall, these results show that soil loss in the experimental subplot was not continuous through time, but occurred in distinct pulses, with a limited number of events contributing a substantial proportion of the annual total.

A comparison of the two monitoring periods suggests that the general pattern of soil loss is event-based, with the highest values associated with specific dates rather than being evenly distributed through time. Even though the first year includes missing observations, both periods show that a relatively small number of events accounted for a large proportion of the total measured soil loss. This behavior highlights the importance of short-term erosive episodes in controlling sediment removal at the subplot scale. Since these measurements were obtained directly in the field, they provide a useful empirical reference for understanding actual soil loss within the monitored area and for comparing plot-scale responses between different hydrological years.

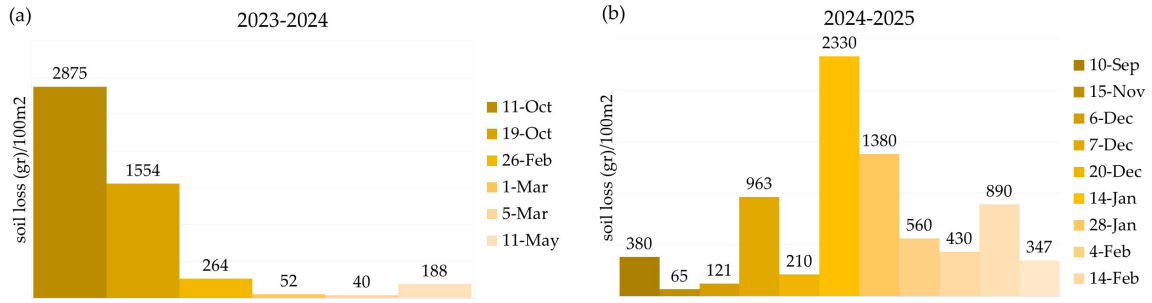

Figure 5. Temporal variation in directly measured soil displacement within the 100 m² experimental subplot for the periods 2023–2024 (a) and 2024–2025 (b).

3.2. RUSLE Model Estimates of Soil Erosion

Rainfall erosivity (R): The R-factor map (Figure 6a) shows that rainfall erosivity is almost uniform across the study sub-catchment. This is expected because the area has a typical

 doi:10.20944/preprints202603.1172.v1

Mediterranean climate, with most rainfall occurring during the wet season and with no major spatial differences over such a small area. Slightly elevated R values appear on the more exposed parts of the catchment, while reduced values occur in the lower-lying areas. This pattern suggests that rainfall intensity may be somewhat greater at higher elevations. Although these differences are not large, they are still important because the R factor directly affects the final soil loss values in the RUSLE model. Therefore, even small increases in R can lead to higher predicted erosion, especially where steep slopes or limited vegetation cover are also present. Overall, the map indicates that rainfall provides a relatively consistent erosive force across the sub-catchment, with only minor local variation.

Soil erodibility (K): The K-factor map (Figure 6b) shows very limited spatial variation across the study sub-catchment, with values remaining close to 0.0249 t·ha·h ha^{-1} MJ^{-1} mm^{-1}. This pattern suggests that soil properties are relatively homogeneous within the selected area. Generally uniform K values are consistent with the dominance of similar calcareous soils developed on comparable parent materials. Even though the spatial variation is small, the overall value indicates that the soils are moderately susceptible to detachment by rainfall and runoff. As a result, where steeper slopes or limited vegetation cover occur, soil erodibility can still contribute substantially to the final erosion estimates.

Slope length and steepness (LS): The LS-factor map (Figure 6d) shows the strongest spatial variability among all RUSLE factors, with values ranging from 0 to about 43.1. The highest values are concentrated along steeper and longer slope segments, where runoff can accumulate and gain erosive energy. In contrast, low LS values occur in flatter parts of the sub-catchment and in short slope sections, where flow concentration is limited. This pattern indicates that topography is a major control on the spatial distribution of erosion risk in the study area. Areas with elevated LS values are expected to experience greater soil loss, especially when combined with sparse vegetation cover or limited support practices.

Cover-management (C): The C-factor map (Figure 6e) presents clear spatial differences related to land cover and management, with values ranging from 0.0623 to 0.2273. Lower C values are associated with areas that have denser vegetation or better ground protection, indicating a lower susceptibility to erosion. By contrast, higher C values occur in more exposed surfaces, including cultivated land or orchard areas with reduced understory cover. This pattern shows that vegetation cover plays an important protective role in the sub-catchment. In practical terms, areas with higher C values are more vulnerable to erosion because the soil surface is less protected against raindrop impact and overland flow.

Support-practice (P): The P-factor map (Figure 6f) varies from approximately 0.206 to 1.749, indicating important spatial differences in the effect of land management and support practices. Lower values represent areas where existing practices reduce runoff and soil loss more effectively, while higher values indicate less protection and therefore greater erosion potential. The observed variation suggests that the influence of support practices is not uniform across the study sub-catchment. In combination with slope and land cover, the P factor helps explain why some parts of the area are more erosion-prone than others, even where rainfall erosivity and soil erodibility remain relatively similar.

 doi:10.20944/preprints202603.1172.v1

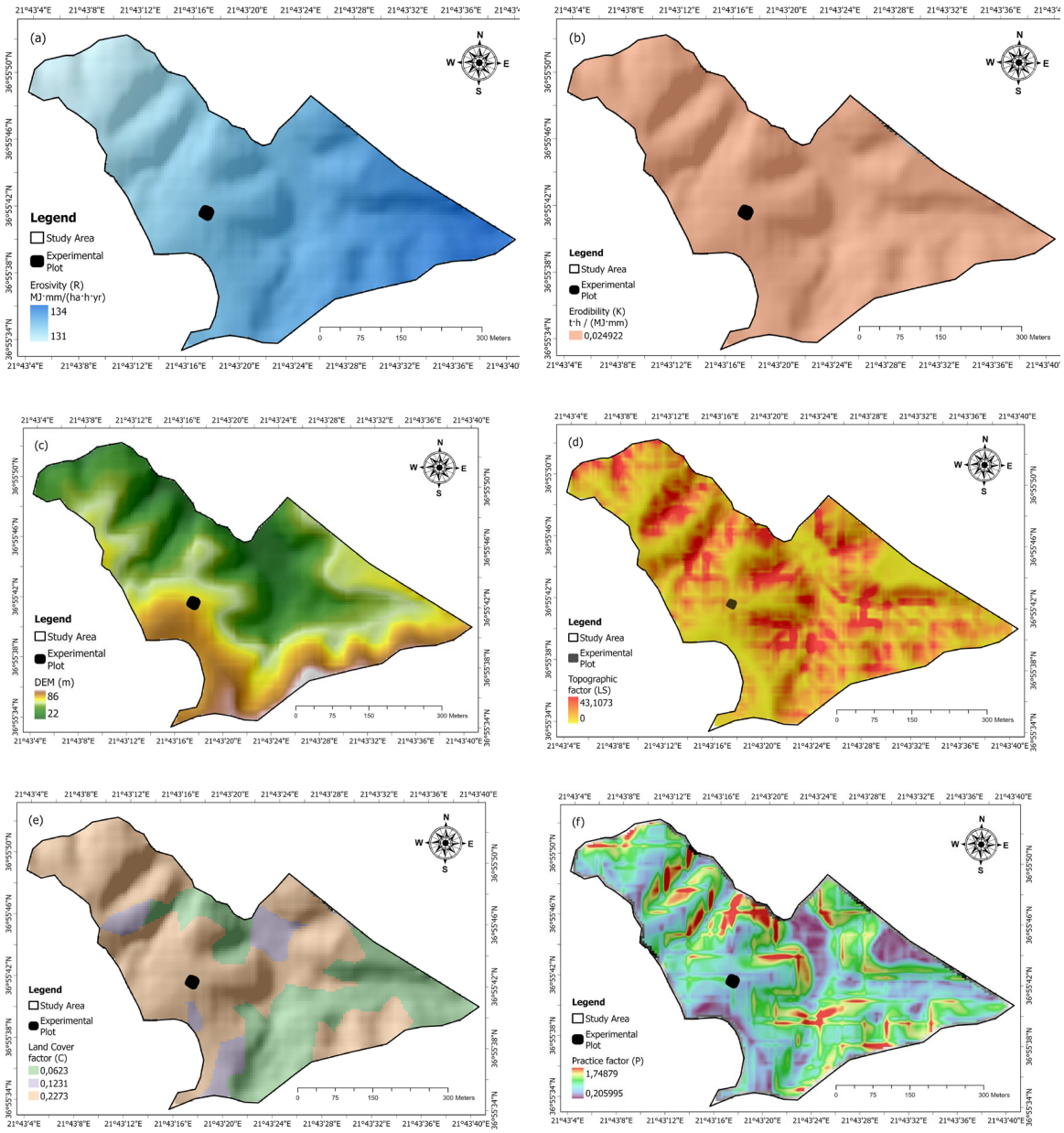

Figure 6. Spatial variability of the RUSLE input factors in the study sub-catchment, including rainfall erosivity (a), soil erodibility (b), elevation (c), topographic factor (d), land cover factor (e), and support practice factor (f).

The final RUSLE soil loss map (Figure 7) shows a clear spatial variation in estimated annual soil erosion across the study sub-catchment. Most of the area falls within the lowest erosion class (0.1–0.5 t ha^{-1} yr^{-1}), indicating generally low to moderate soil loss under the present environmental and land-use conditions. However, several distinct zones of increased erosion risk are visible, mainly in the central, northwestern, and southeastern parts of the sub-catchment, where soil loss values rise to 1.3–3.2 t ha^{-1} yr^{-1}, and locally reach the highest class of 3.3–6.1 t ha^{-1} yr^{-1}. These hotspots are likely associated with the combined effect of steeper slopes, greater flow concentration, reduced vegetation cover, and less effective support practices. In contrast, the more stable areas with lower predicted soil loss appear to correspond to gentler terrain and surfaces with better protective cover. The map therefore highlights that soil erosion is not uniformly distributed within the study area but is concentrated in specific parts of the landscape where topographic and land management conditions enhance runoff and sediment detachment. Overall, the results suggest that although the sub-catchment is relatively small, it contains localized erosion-prone areas that may require targeted soil conservation measures.

 doi:10.20944/preprints202603.1172.v1

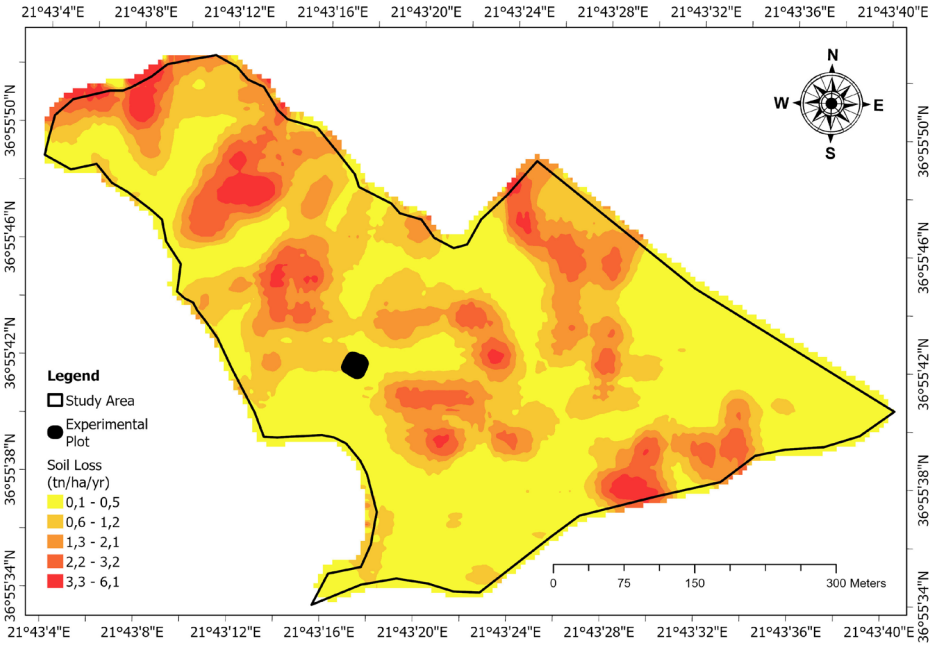

Figure 7. Spatial distribution of predicted annual soil loss in the study sub-catchment based on the RUSLE model.

3.3. Terrain Elevation Change (DEM of Difference)

To better understand short-term changes in the soil surface, a DEM of Difference (DoD) approach was applied to the experimental plot using multitemporal elevation data. In this study, the DoD analysis was used to identify patterns of surface displacement and soil movement between survey dates, rather than to directly quantify soil loss. For this reason, the first step focused on producing a reliable bare-earth representation of the plot by removing vegetation from the LiDAR-derived surface model. The comparison between the original and filtered DEMs illustrates the importance of this processing step.

In Figure 8a, the unprocessed LiDAR surface still includes vegetation canopy, which appears as elevated and irregular peaks across the plot. These features mask the actual terrain and reduce the visibility of the underlying ground morphology. In Figure 8b, after vegetation filtering, the surface becomes clearer and more continuous, allowing the main topographic characteristics of the plot to be identified more effectively. In particular, the general slope pattern, terrace-like elements, shallow depressions, and small flow paths become more visible in the filtered DEM. Although the total elevation difference across the plot is relatively small, on the order of a few meters, the removal of vegetation greatly improves the representation of microtopographic detail. This step was therefore essential for the subsequent DoD analysis, as it provided the terrain model needed to interpret local surface changes on the actual ground surface.

 doi:10.20944/preprints202603.1172.v1

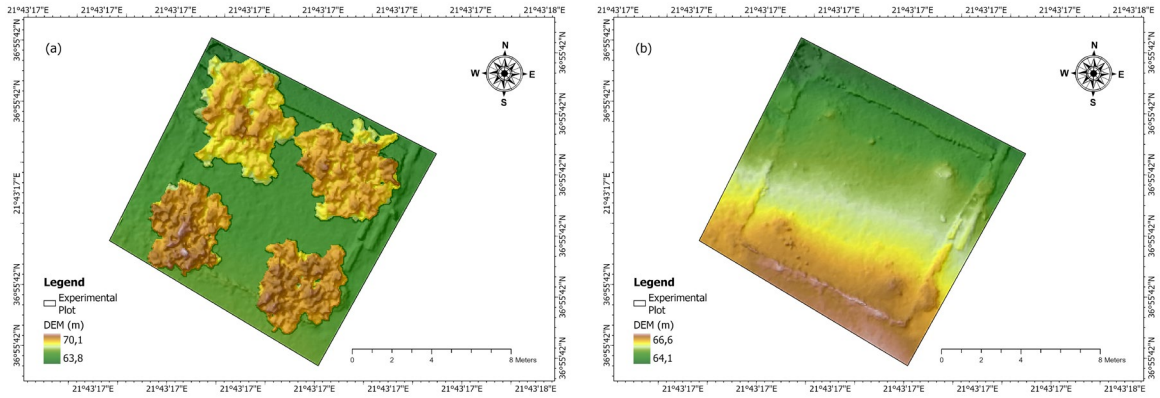

Figure 8. Lidar-derived surface elevation before and after vegetation filtering. (a) Raw point-cloud DEM (tree tops and ground vegetation still present). (b) Filtered ground DEM (vegetation removed).

The comparison between the DEMs acquired in December 2024 (Figure 9a) and May 2025 (Figure 9b) provides an initial view of how the soil surface evolved during the monitoring period. In both datasets, the general topographic structure of the experimental plot remains consistent, with the main slope direction and the overall terrain pattern clearly preserved. At the same time, some local differences can be observed between the two dates, especially in small-scale surface features and in the spatial distribution of elevation values across the plot. These variations suggest that the surface did not remain static but underwent localized changes over time.

In the December 2024 DEM, the surface appears relatively smoother in some parts of the plot, whereas the May 2025 DEM shows a more pronounced expression of microtopographic features in specific areas. Such differences may indicate zones where material was redistributed along the slope or where the soil surface was slightly reworked between surveys. For this reason, the comparison of the two DEMs is useful as a first step in identifying spatial patterns of terrain change before calculating the DEM of Difference. Rather than being interpreted directly as soil loss, these temporal differences are better understood as indicators of surface displacement and local soil movement, which can then be examined more clearly through the DoD analysis.

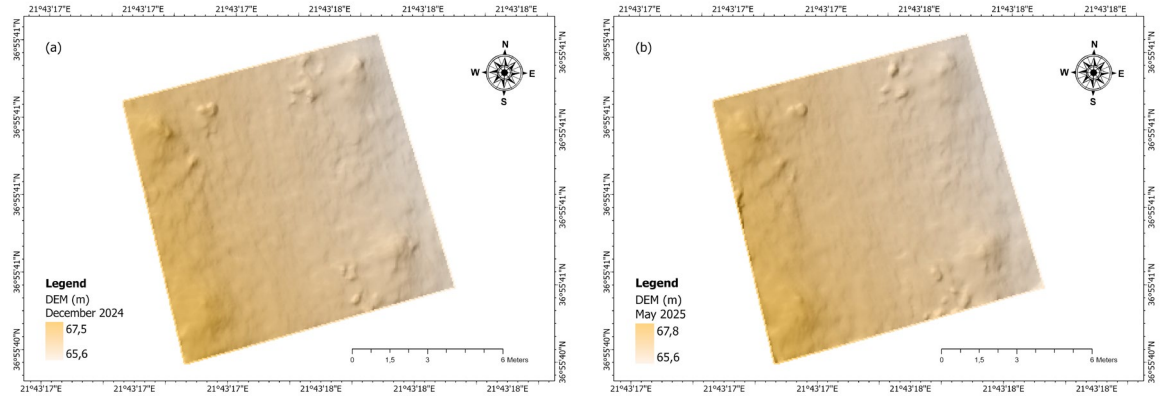

Figure 9. Bare-earth digital elevation models (DEMs) of the experimental plot for December 2024 (a) and May 2025 (b).

The DoD map (Figure 10) reveals a spatially variable pattern of surface elevation change across the experimental plot between December 2024 and May 2025. Both positive and negative changes are present, showing that the soil surface was affected by localized redistribution processes during the monitoring period. Areas with negative elevation change indicate zones where the surface became lower, while positive elevation change mark areas where material appears to have accumulated or where the surface became relatively higher.

 doi:10.20944/preprints202603.1172.v1

The observed pattern is not uniform, but rather dispersed across the plot, with some clusters of change appearing along microtopographic irregularities and small flow pathways. This suggests that short-term surface dynamics were controlled by local terrain conditions and by the movement of material over short distances within the plot. In this study, the DoD results are interpreted primarily as indicators of soil displacement and surface movement, rather than as a direct measure of soil loss. Therefore, the map is useful for identifying where the soil surface was more active during the observation period and for understanding the spatial distribution of local terrain adjustments.

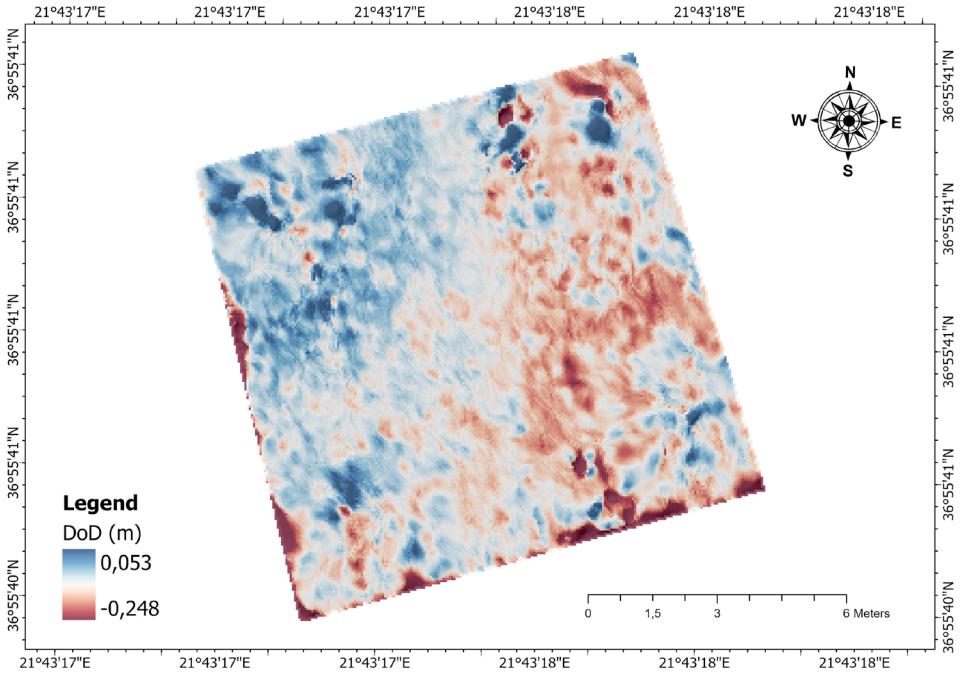

Figure 10. DEM of Difference (DoD) of the experimental plot showing surface elevation changes between December 2024 and May 2025.

4. Discussion

The main strength of this study is that soil erosion was examined using a multi-method approach, combining direct field measurements, RUSLE modelling, and LiDAR/DoD-based surface analysis. This is important because soil erosion is a complex process [40] influenced by multifactorial factors [41] acting across different spatial and temporal scales; therefore, a single method is rarely sufficient to capture its full behavior. Recent studies from Mediterranean environments show that runoff plots provide direct field evidence of sediment loss, while GIS- and remote sensing-based models represent the spatial distribution of erosion risk; together, these approaches offer a more complete understanding of erosion processes [42,43]. Runoff plots are especially valuable because they provide direct event-scale measurements of gross soil loss [7,44], while RUSLE offers spatially distributed predictions of erosion risk [17,45,46], and DoD methods [47] help visualize how the soil surface changes through time.

Among the methods tested, the field experiment provided the most direct evidence of actual soil loss from the monitored subplot [43,48]. Well-installed runoff plots are widely regarded as one of the most reliable field approaches for quantifying soil removed from a defined area, particularly because they can record the response to individual rainfall events at high temporal resolution. At the same time, their usefulness depends strongly on the quality of installation, maintenance, and continuity of measurements. In our case, the field data gave a clear picture of event-driven soil loss, but the first monitoring year included some gaps caused by technical problems in the collection system. These missing observations are acknowledged as a limitation; however, the missing period did not coincide

 doi:10.20944/preprints202603.1172.v1

with intense rainfall, and therefore it is unlikely that major soil-loss events were missed. Even with this constraint, the field experiment remains the most direct reference dataset in the study because it reflects measured soil export from the 100 m^2 subplot rather than modelled or inferred change.

The RUSLE results showed good agreement with the field measurements once the comparison was made at the appropriate spatial scale. This is one of the most important outcomes of this study. The measured annual soil loss values of 0.497 t ha^{-1} for 2023–2024 and 0.768 t ha^{-1} for 2024–2025 fall within, or very close to, the 0.6–1.2 t ha^{-1} yr^{-1} range predicted by RUSLE for the pixels corresponding to the experimental plot. This does not mean that the two approaches are identical, but it does indicate that they are in the same order of magnitude and that the model reproduced the local erosion signal reasonably well. This agreement is particularly meaningful because RUSLE is one of the most widely used empirical models for estimating soil erosion [19], yet its performance depends strongly on the quality of the input layers used to derive the R, K, LS, C, and P factors [28]. Reliable RUSLE predictions require well-prepared input data and, whenever possible, independent validation against field observation [22,49]. In the present study, the quality of the local input data was high, and this likely explains why the model outputs were consistent with the measured plot-scale values.

This also helps justify the decision to apply RUSLE to a small, well-defined sub-catchment rather than to the entire Xerias watershed. RUSLE was originally developed for estimating long-term average annual soil loss [28] and is generally more defensible when applied at plot to small-catchment scales [50], especially when local information is available for parameterization and some form of field validation is possible. When the model is transferred to larger areas without validation, uncertainty increases because the input factors become more generalized and because deposition processes are not explicitly represented [17]. In that respect, our study contributes by showing that a sub-catchment-scale application linked to direct field measurements can produce realistic erosion estimates under Mediterranean olive-growing conditions. The contribution is therefore not only the map itself, but also the demonstration that local validation improves confidence in the mapped results.

The LiDAR and DoD analysis added a different but complementary perspective. Unlike runoff plots, which measure exported sediment, the DoD approach mainly reveals surface elevation change [51], allowing the identification of zones where the soil surface was lowered or raised between surveys. For this reason, in the present work the DoD results are interpreted primarily in terms of soil displacement and local surface redistribution, rather than as a direct estimate of soil loss. This interpretation is consistent with other DoD-based studies, which show that differenced DEMs are particularly effective for mapping where topographic change occurs and for identifying short-distance redistribution patterns across small plots and hillslopes [52]. In our plot, the DoD pattern supports the general expectation that material tends to move from relatively higher to relatively lower positions, indicating downslope redistribution of soil within the monitored surface.

At the same time, the DoD part of the study should be interpreted as an exploratory but promising component of the overall methodology. The monitored area was relatively small (100 m^2), and the comparison covered only a five-month period, which limits the degree to which broader or longer-term erosion patterns can be inferred. In addition, the usefulness of DoD products depends strongly on the quality of the DEMs and on their spatial resolution, because high-resolution surfaces are needed to preserve microtopographic features that control flow concentration and local erosion. Previous UAV- and LiDAR-based studies have shown that DEM resolution has a strong influence on slope representation, LS estimation, and the visibility of microtopographic change [53,54]. For that reason, the DoD results in this study are best viewed as a detailed indicator of surface behaviour at plot scale, rather than as a stand-alone measure of annual soil loss. Even so, they are valuable because they reveal the internal spatial organization of terrain change in a way that neither runoff plots nor RUSLE can show on their own.

Taken together, the three approaches show that soil erosion assessment benefits from a holistic framework. The field experiment supplies direct measurements, RUSLE provides spatial extrapolation and identifies erosion-prone areas, and LiDAR/DoD reveals fine-scale redistribution of

 doi:10.20944/preprints202603.1172.v1

the soil surface. This combination responds to a common limitation in erosion research, namely that many studies rely on only one method and therefore capture only one dimension of the process. Recent Mediterranean reviews explicitly call for this kind of multi-method, multi-scale strategy, because each method provides only a partial but useful view of erosion dynamics. Our work contributes to this discussion by showing that, even in a relatively small Mediterranean sub-catchment, an integrated design can link direct observations with spatial modelling and high-resolution terrain analysis. Future work can build on this framework by extending monitoring duration, enlarging the number of plots, and further refining terrain-based analysis, with the aim of reducing remaining limitations and strengthening comparisons among methods.

5. Conclusions

This study showed that soil erosion assessment in Mediterranean olive-growing areas can be improved through the combined use of direct field measurements, RUSLE modelling, and LiDAR-based terrain analysis. The field experiment provided direct evidence of actual soil loss at the subplot scale, while the RUSLE model offered a spatially distributed estimate of erosion risk across the study sub-catchment. The agreement between the measured annual soil loss values and the RUSLE-predicted range at the experimental plot suggests that, when supported by high-quality local input data, RUSLE can provide realistic estimates of soil erosion under local conditions.

The LiDAR–DoD approach contributed an additional and complementary perspective by identifying short-term changes in surface elevation and patterns of local soil redistribution within the experimental plot. Although this method was not used here as a direct measure of soil loss, it proved useful for describing soil displacement and surface behavior over time. Taken together, the three approaches showed that soil erosion is a complex process that cannot be fully captured by a single method, and that a multi-method framework can support a more complete understanding of erosion dynamics.

Overall, the findings highlight the importance of integrated erosion assessment not only for estimating soil loss, but also for improving our understanding of land degradation processes in vulnerable Mediterranean agroecosystems. Since soil erosion is one of the main drivers of land degradation, especially in sloping cultivated areas, the combined methodology applied in this study may support more targeted soil conservation and sustainable land management strategies. Future research should further refine these approaches, reduce remaining limitations, and expand monitoring in order to strengthen erosion assessment at both plot and sub-catchment scales.

Author Contributions: Conceptualization, C.P. and P.T.N.; methodology, C.P. and P.T.N.; software, C.P. and P.T.N.; validation, C.P. and P.T.N.; formal analysis, C.P. and P.T.N.; investigation, C.P. and P.T.N.; resources, C.P. and P.T.N.; data curation, C.P. and P.T.N.; writing—original draft preparation, C.P.; writing—review and editing, P.T.N.; visualization, C.P. and P.T.N.; supervision, P.T.N.; project administration, C.P. and P.T.N.; funding acquisition, P.T.N. All authors have read and agreed to the published version of the manuscript.

Funding: This research received no external funding.

Data Availability Statement: The original contributions presented in this study are included in the article. Further enquiries can be directed to the corresponding authors.

Acknowledgments: The authors would like to acknowledge the Navarino Environmental Observatory (NEO) for supporting this work through the provision of facilities and research infrastructure. We also thank Costa Navarino for providing meteorological data from its monitoring network, which contributed to the implementation of this study.

Conflicts of Interest: The authors declare no conflicts of interest.

Abbreviations

The following abbreviations are used in this manuscript:

 doi:10.20944/preprints202603.1172.v1

RUSLE	Revised Universal Soil Loss Equation
DEM	Digital Elevation Model
DoD	DEM of Difference
LiDAR	Light Detection and Ranging
GIS	Geographic Information System(s)
OM	Organic Matter
RTK	Real-time kinematic positioning

References

1. Li, L.; Du, S.; Wu, L.; Liu, G. An Overview of Soil Loss Tolerance. *CATENA* **2009**, *78*, 93–99, doi:https://doi.org/10.1016/j.catena.2009.03.007.
2. Carr, T.W.; Balkovič, J.; Dodds, P.E.; Folberth, C.; Skalský, R. The Impact of Water Erosion on Global Maize and Wheat Productivity. *Agric. Ecosyst. Environ.* **2021**, *322*, doi:https://doi.org/10.1016/j.agee.2021.107655.
3. Andualem, T.G.; Hewa, G.A.; Myers, B.R.; Peters, S.; Boland, J. Erosion and Sediment Transport Modeling: A Systematic Review. *Land* **2023**, *12*, 1396, doi:https://doi.org/10.3390/land12071396.
4. Guerra, C.A.; Rosa, I.M.D.; Valentini, E.; Wolf, F.; Rosa, I.M.D.; Filipponi, F.; Karger, D.N.; Xuan, A.N.; Mathieu, J.; Lavelle, P.; et al. Global Vulnerability of Soil Ecosystems to Erosion. *Landscape Ecol.* **2020**, *35*, 823–842, doi:https://doi.org/10.1007/s10980-020-00984-z.
5. García-Ruiz, J.M.; Nadal-Romero, E.; Lana-Renault, N.; Beguería, S. Erosion in Mediterranean Landscapes: Changes and Future Challenges. *Geomorph.* **2013**, *198*, 20–36, doi:https://doi.org/10.1016/j.geomorph.2013.05.023.
6. Samela, C.; Imbrenda, V.; Coluzzi, R.; Pace, L.; Simoniello, T.; Lanfredi, M. Multi-Decadal Assessment of Soil Loss in a Mediterranean Region Characterized by Contrasting Local Climates. *Land* **2022**, *11*, 1010, doi:https://doi.org/10.3390/land11071010.
7. A. Peñuela; González-Sánchez, E.J.; Milazzo, F. Soil Erosion in Mediterranean Olive Groves: A Review. *Soil* **2026**, *12*, 93–111, doi:https://doi.org/10.5194/soil-12-93-2026.
8. Scholten, T.; Seitz, S. Soil Erosion and Land Degradation. *Soil Syst.* **2019**, *3*, 68, doi:https://doi.org/10.3390/soilsystems3040068.
9. Ferreira, C.S.S.; Seifollahi-Aghmiuni, S.; Destouni, G.; Ghajarnia, N.; Kalantari, Z. Soil Degradation in the European Mediterranean Region: Processes, Status and Consequences. *Sci. Total Environ.* **2022**, doi:10.1016/j.scitotenv.2021.150106. Epub 2021 Sep 4.
10. Gomez, J.A.; Amato, M.; Celano, G.; Koubouris, G.C. Organic Olive Orchards on Sloping Land: More than a Specialty Niche Production System? *J. Environ. Manage.* **2008**, *89*, 99–109, doi:10.1016/j.jenvman.2007.04.025.
11. Deitch, M.J.; Sapundjieff, M.J.; Feirer, S.T. Characterizing Precipitation Variability and Trends in the World's Mediterranean-Climate Areas. *Water* **2017**, *9*, 259, doi:https://doi.org/10.3390/w9040259.
12. Vaezi, A.R.; Ahmadi, M.; Cerdà, A. Contribution of Raindrop Impact to the Change of Soil Physical Properties and Water Erosion under Semi-Arid Rainfalls. *Sci. Total Environ.* **2017**, *583*, 382–392, doi:https://doi.org/10.1016/j.scitotenv.2017.01.078.
13. Márquez-García, F.; Hayas, A.; Peña, A.; Ordóñez-Fernández, R.; González-Sánchez, E.J. Influence of Cover Crops and Tillage on Organic Carbon Loss in Mediterranean Olive Orchards. *Soil Till. Res.* **2024**, *235*, doi:https://doi.org/10.1016/j.still.2023.105905.
14. Chontos, K.; Pantazis, C.; Berg, H. Impact of Soil Management Practices on Olive Orchard Soil Health and Arthropod Diversity in Messenia, Greece. *Agronomy* **2026**, *16*, 404, doi:https://doi.org/10.3390/agronomy16040404.
15. González-Rosado, M.; Parras-Alcántara, L.; Aguilera-Huertas, J.; Lozano-García, B. Soil Productivity Degradation in a Long-Term Eroded Olive Orchard under Semiarid Mediterranean Conditions. *Agronomy* **2021**, *11*, 812, doi:https://doi.org/10.3390/agronomy11040812.

 doi:10.20944/preprints202603.1172.v1

16. Boix-Fayos, C.; Martínez-Mena, M.; Arnau, E.; Calvo-Cases, A.; Castillo, V.; Albaladejo, J. Measuring Soil Erosion by Field Plots: Understanding the Sources of Variation. *Earth-Science Reviews* **2006**, *78*, 267–285, doi:10.1016/j.earscirev.2006.05.005.
17. Räsänen, T.A.; Tähtikarhu, M.; Uusi-Kämppä, J.; Piirainen, S.; Turtola, E. Evaluation of RUSLE and Spatial Assessment of Agricultural Soil Erosion in Finland. *Geoderma Reg.* **2023**, *32*, doi:https://doi.org/10.1016/j.geodrs.2023.e00610.
18. Alexiou, S.; Papanikolaou, I.; Schneiderwind, S.; Kehrle, V.; Reicherter, K. Monitoring and Quantifying Soil Erosion and Sedimentation Rates in Centimeter Accuracy Using UAV-Photogrammetry, GNSS, and t-LiDAR in a Post-Fire Setting. *Remote Sens.* **2024**, *16*, 802, doi:https://doi.org/10.3390/rs16050802.
19. Benavidez, R.; Jackson, B.; Maxwell, D.; Norton, K. A Review of the (Revised) Universal Soil Loss Equation ((R)USLE): With a View to Increasing Its Global Applicability and Improving Soil Loss Estimates. *Hydrol. Earth Syst. Sci* **2018**, 6059–6086, doi:https://doi.org/10.5194/hess-22-6059-2018.
20. Renard, K.G.; Foster, G.R.; Weesies, G.A.; Porter, J.P. RUSLE: Revised Universal Soil Loss Equation. *J. Soil Water Conserv.* **1991**, *46*, 30–33.
21. Abdelsamie, E.A.; Abdellatif, M.A.; Hassan, F.O.; El Baroudy, A.A.; Mohamed, E.S.; Kucher, D.E.; Shokr, M.S. Integration of RUSLE Model, Remote Sensing and GIS Techniques for Assessing Soil Erosion Hazards in Arid Zones. *Agriculture* **2023**, *13*, 35, doi:https://doi.org/10.3390/agriculture13010035.
22. Ganasri, B.P.; Ramesh, H. Assessment of Soil Erosion by RUSLE Model Using Remote Sensing and GIS - A Case Study of Nethravathi Basin. *Geoscience Frontiers* **2016**, *7*, 953–961, doi:https://doi.org/10.1016/j.gsf.2015.10.007.
23. Batista, P.V.G.; Davies, J.; Silva, M.L.N.; Quinton, J.N. On the Evaluation of Soil Erosion Models: Are We Doing Enough? *Earth-Science Reviews* **2019**, *197*, doi:https://doi.org/10.1016/j.earscirev.2019.102898.
24. Ta, N.; Wang, C.; Zhao, S.; Zhang, Q. Quantifying Soil Erosion Processes Based on Micro-ΔDEM. *Water* **2025**, *17*, 2557, doi:https://doi.org/10.3390/w17172557.
25. Kakkavou, K.; Gemtou, M.; S. Fountas Drivers and Barriers to the Adoption of Precision Irrigation Technologies in Olive and Cotton Farming—Lessons from Messenia and Thessaly Regions in Greece. *Smart Agr. Technol.* **2024**, *7*, doi:https://doi.org/10.1016/j.atech.2024.100401.
26. Thanopoulos, R.; Drossinou, I.; Koutroumpelas, I.; Chatzigeorgiou, T.; Stavrakaki, M.; Bebeli, P.J. Hilly, Semi-Mountainous and Mountainous Areas Harbor Landraces Diversity: The Case of Messinia (Peloponnese-Greece). *Diversity* **2024**, *16*, 151, doi:https://doi.org/10.3390/d16030151.
27. Pantazis, C.; Solomos, S.; Nastos, P.; Maneas, G.; Kairis, O.; Centrito, M.; Marino, G.; Roggero, P.P.; Mihail, J.; Fountoulakis, I.; et al. Insights into the Effects of Climate Variability and Agricultural Practices on Olive Orchards in Messenia, Greece: A Field Experiment Study. *SSRN Preprint* **2025**.
28. Wischmeier, W.H.; Smith, D.D. Predicting Rainfall Erosion Losses, a Guide to Conservation Planning. *U.S. Department of Agriculture: Washington, DC, USA* **1978**, 62.
29. Renard, K.G.; Foster, G.R.; Weesies, G.A.; McCool, D.K.; Yoder, D.C. Predicting Soil Erosion by Water: A Guide to Conservation Planning with the Revised Universal Soil Loss Equation. *USDA Agric.* **1996**.
30. Renard, K.G.; Freimund, J.R. Using Monthly Precipitation Data to Estimate the R-Factor in the Revised USLE. *J. Hydrol.* **1994**, 287–306, doi:https://doi.org/10.1016/0022-1694(94)90110-4.
31. Arnoldus, H.M.J. An Approximation of the Rainfall Factor in the Universal Soil Loss Equation. *John Wiley and Sons: Chichester, UK,* **1980**.
32. Fournier, F. Climat et EÉrosion. *Presses Universitaires: Paris, France* **1960**.
33. Arnoldus, J.M.J. Methodology Used to Determine the Maximum Potential Average Annual Soil Loss Due to Sheet and Rill Erosion in Morocco. *Food Agric. Org. Soils Bull.* **1977**, 39–51.
34. Moore, I.D.; Burch, G.J. Physical Basis of the Length-Slope Factor in the Universal Soil Loss Equation. *Soil Sci. Soc. Am. J.* **1986**, *50*, 1294–1298, doi:https://doi.org/10.2136/sssaj1986.03615995005000050042x.
35. Moore, I.D.; Wilson, J.P. Length-Slope Factors for the Revised Universal Soil Loss Equation: Simplified Method of Estimation. *J. Soils Water Conserv.* **1992**, *47*, 423–428.
36. P. Panagos; P. Borrelli; K. Meusburger; C. Alewell; E. Lugato; L. Montanarella Estimating the Soil Erosion Cover-Management Factor at the European Scale. *Land Use Policy* **2015**, *48*, 38–50, doi:http://dx.doi.org/10.1016/j.landusepol.2015.05.021.

 doi:10.20944/preprints202603.1172.v1

37. Anders, N.; Valente, J.; Masselink, R.; Keesstra, S. Comparing Filtering Techniques for Removing Vegetation from UAV-Based Photogrammetric Point Clouds. *Drones* **2019**, *3*, 61, doi:https://doi.org/10.3390/drones3030061.
38. Storch, M.; Kisliuk, B.; Jarmer, T.; Waske, B.; Lange, N. de Comparative Analysis of UAV-Based LiDAR and Photogrammetric Systems for the Detection of Terrain Anomalies in a Historical Conflict Landscape. *Sci. Remote Sens.* **2025**, *11*, doi:https://doi.org/10.1016/j.srs.2024.100191.
39. Wheaton, J.M.; Brasington, J.; Darby, S.E.; Sear, D.A. Accounting for Uncertainty in DEMs from Repeat Topographic Surveys: Improved Sediment Budgets. *Earth Surf. Process. Landforms* **2009**, *35*, 136–156, doi:https://doi.org/10.1002/esp.1886.
40. Wen, X.; Deng, X. Current Soil Erosion Assessment in the Loess Plateau of China: A Mini-Review. *J. Clean. Prod.* **2020**, *276*, doi:https://doi.org/10.1016/j.jclepro.2020.123091.
41. Epple, L.; Kaiser, A.; Schindewolf, M.; Bienert, A.; Lenz, J.; Eltner, A. A Review on the Possibilities and Challenges of Today's Soil and Soil Surface Assessment Techniques in the Context of Process-Based Soil Erosion Models. *Remote Sens.* **2022**, *14*, 2468, doi:https://doi.org/10.3390/rs14102468.
42. Alexakis, D.D.; Hadjimitsis, D.G.; Agapiou, A. Integrated Use of Remote Sensing, GIS and Precipitation Data for the Assessment of Soil Erosion Rate in the Catchment Area of "Yialias" in Cyprus. *Atmos. Res.* **2013**, *131*, 108–124, doi:https://doi.org/10.1016/j.atmosres.2013.02.013.
43. Pantazis, C.; Nastos, P. Comparing Direct Field Measurements of Soil Erosion with RUSLE Model Estimates in Mediterranean Olive Orchards. *Environ. Earth Sci. Proc.* **2025**, *35*, 75, doi:https://doi.org/10.3390/eesp2025035075.
44. Maetens, W.; Poesen, J.; Vanmaercke, M. How Effective Are Soil Conservation Techniques in Reducing Plot Runoff and Soil Loss in Europe and the Mediterranean? *Earth-Sci. Rev.* **2012**, *115*, 21–36, doi:https://doi.org/10.1016/j.earscirev.2012.08.003.
45. Thapa, P. Spatial Estimation of Soil Erosion Using RUSLE Modeling: A Case Study of Dolakha District, Nepal. *Environ. Syst. Res.* **2020**, *9*, doi:https://doi.org/10.1186/s40068-020-00177-2.
46. Zaied, M.B.; Jomaa, S.; Ouessar, M. Soil Erosion Estimates in Arid Region: A Case Study of the Koutine Catchment, Southeastern Tunisia. *Appl. Sci.* **2021**, *11*, 6763, doi:https://doi.org/10.3390/app11156763.
47. Nastos, P.; Pantazis, C.; Solomos, S.; Fountoulakis, I.; Zerefos, C.S. Evaluating Soil Erosion Risk in Olive Orchards through Drone-Based Monitoring and Field Experiments. *Eleventh International Conference on Remote Sensing and Geoinformation of the Environment (RSCy2025), 2025, Paphos, Cyprus*, doi:https://doi.org/10.1117/12.3075485.
48. Critchley, W.; Siegert, K. *A Manual for the Design and Construction of Water Harvesting Schemes for Plant Production*; Food and Agriculture Organization of the United Nations: Rome, 1991;
49. USDA Agricultural Research Service *Predicting Soil Erosion by Water: A Guide to Conservation Planning with the Revised Universal Soil Loss Equation (RUSLE)*; United States Department of Agriculture: Washington, DC, 1997;
50. Terefe, B.; Melese, T.; Tsegaye, A.; Afework, A.; Yibeltal, T.; Anagaw, A.; Temesgen, F.; Belay, T.; Assefa, G.; Mencho, B.B. Soil Loss Estimation in Ethiopia: A Comprehensive Review of the RUSLE Model Integrated with Geospatial Technologies. *Discov. Sustain.* **2025**, *6*, 334, doi:https://doi.org/10.1007/s43621-025-01037-8.
51. Anders, N.; Valente, J.; Masselink, R.; Keesstra, S. Comparing Filtering Techniques for Removing Vegetation from UAV-Based Photogrammetric Point Clouds. *Drones* **2019**, *3*, 61, doi:https://doi.org/10.3390/drones3030061.
52. Richard, W. DEMs of Difference. *Geomorphological Techniques* **2012**.
53. Chidi, C.L.; Zhao, W.; Chaudhary, S.; Xiong, D.; Wu, Y. Sensitivity Assessment of Spatial Resolution Difference in DEM for Soil Erosion Estimation Based on UAV Observations: An Experiment on Agriculture Terraces in the Middle Hill of Nepal. *ISPRS Int. J. Geo-Inf.* **2021**, *10*, 28, doi:https://doi.org/10.3390/ijgi10010028.
54. W. Dai; Hu, J.; Wang, B.; Fan, M.; Zhou, Y.; Zhang, M. Effects of Digital Elevation Model Resolution on Unmanned Aerial Vehicle-Based Topographic Change Detection in Human-Altered Landscapes. *Drones* **2024**, *8*, 610, doi:https://doi.org/10.3390/drones8110610.

 doi:10.20944/preprints202603.1172.v1